Nanoscale Res Lett (2010) 5:7–13
DOI 10.1007/s11671-009-9434-3

NANO EXPRESS

Probing Nucleation Mechanism of Self-Catalyzed InN Nanostructures

Guowei Xu · Zhuangzhi Li · Javier Baca · Judy Wu

Received: 3 June 2009 / Accepted: 2 September 2009 / Published online: 16 September 2009

Abstract The nucleation and evolution of InN nanowires in a self-catalyzed growth process have been investigated to probe the microscopic growth mechanism of the self-catalysis and a model is proposed for high pressure growth window at ~760 Torr. In the initial stage of the growth, amorphous InN_x microparticles of cone shape in liquid phase form with assistance of an InN_x wetting layer on the substrate. InN crystallites form inside the cone and serve as the seeds for one-dimensional growth along the favorable [0001] orientation, resulting in single-crystalline InN nanowire bundles protruding out from the cones. An amorphous InN_x sheath around the faucet tip serves as the interface between growing InN nanowires and the incoming vapors of indium and nitrogen and supports continuous growth of InN nanowires in a similar way to the oxide sheath in the oxide-assisted growth of other semiconductor nanowires. Other InN 1D nanostructures, such as belts and tubes, can be obtained by varying the InN crystallites nucleation and initiation process.

Keywords Indium nitride · Self-catalyzed · Nanowires · InN_x cones · Sheath

Introduction

Indium nitride (InN) is currently receiving much attention, in large part due to its recently observed narrow band gap E_g of 0.7–0.9 eV [1–3]. The direct band-gap transition in InN and its ability to form ternary (ex. InGaN) and quaternary (ex. AlInGaN) alloys increases the versatility of group-III nitride in optoelectronic devices in a broad spectrum ranging from near IR to UV. InN also has promising transport and electronic properties. It has the smallest effective electron mass of all the group-III nitrides, which leads to high mobility and high saturation velocity, and a large drift velocity at room temperature [4–7]. In the form of one-dimensional (1D) nanostructures such as nanowires and nanotubes [8, 9], the dimension effect of either quantum or classical origin provides further tune on the physical properties of the InN including energy band and electrical charge transport. This has generated considerable interests in growth of InN 1D nanostructures and exciting progress has been made recently [10–14].

Unlike in growth of many other semiconductor nanowires where a metal catalyst plays a critical role in nucleation, initiation, and definition of lateral dimension of 1D nanostructures in vapor–liquid-solid (VLS) growth [15–17], most reported InN nanowire growth claims a self-catalysis growth mechanism using either vapor transport or reactive vapor transport of indium onto substrates in the presence of decomposed ammonia [11, 18, 19]. This is partly due to the low decomposition temperature of InN around ~600 °C, making selection of the metal catalysts of low eutectic point and high solubility for nitrogen difficult. In fact, self-catalysis may be advantageous for device applications by eliminating metal catalyst contamination. Understanding the microscopic mechanism of the self-catalysis is therefore of primary importance toward controlled growth of InN nanostructures with desired physical properties including morphology, lateral dimension, orientation, crystalline structure. Disappointedly, the microscopic mechanism of the self-catalysis is barely understood so far. Although indium condensation on the substrate was argued to possibly assist nucleation of the

G. Xu (✉) · Z. Li · J. Baca · J. Wu
Department of Physics and Astronomy, University of Kansas, Lawrence, KS 66045, USA
e-mail: xgw@ku.edu

InN nanowire [11, 18, 19], it remains unclear how the nucleation occurs at a microscopic scale, how the 1D growth initiates and evolves, and what determines the nanowire geometry and dimension. In this work, an attempt was made to probe initial growth stage of the InN nanowires in a chemical vapor deposition (CVD) process. Strikingly, we observed single-crystalline [0001] oriented InN nanowire bundles initiated from amorphous InN_x microcones formed at the early stage of the growth. In this paper, we present our experimental results and a model based on the observation to explain the self-catalytic growth of the 1D InN nanostructures.

Experiment

The growth of InN nanowires was carried out in a home-designed CVD system using metal indium (99.999%) and high purity ammonia (99.999%) as the sources. This CVD chamber has a unique gas feeding system fitted snuggly into a small quartz tube (growth chamber with indium source and sample inside), allowing local overpressure when the downstream end of the quartz tube was partially blocked. The inner diameter of the quartz tube is 7 mm and the length is 250 mm. Prior to each growth run, the indium source was cleaned using dilute nitric acid and DI water to remove native oxide layer on the surface. It was then placed inside the small quartz tube at the center of a tube furnace to reach the desired growth temperature based on the furnace temperature calibration curve. The samples were placed downstream at a selected distance from the indium source. Before growth, the CVD system was pumped to $\sim$20 mTorr followed by purge with N_2 for 2 min and this process was typically repeated for three times. Ammonia was then flowed into the growth chamber at 16 SCCM (standard cubic centimeter) as the temperature of the furnace was ramped to the growth temperature in the range of 650–850 °C (or indium source temperature) at 10 °C/min and maintained for up to 5 h during InN growth. The system was then rapidly cooled down to room temperature under ammonia flow. Different chamber pressures in the range from 10 to 760 Torr were examined by controlling the pumping rate. The InN nanostructures were collected from the surface of Si (111) substrates placed at 11.5–15.0 cm away from the indium source. The sample growth temperature was typically 110–320 °C lower than the indium source temperature depending on the sample-to-source distance. The morphology and microstructure of the InN nanostructures were characterized using scanning electron microscopy (SEM) and transmission electron microscopy (TEM). X-ray diffraction (XRD) spectra were collected for phase determination and energy dispersive X-ray spectroscopy (EDS) analysis for component confirmation. The semiconductor band-gap energy E_g of the sample was investigated using Fourier Transform Infrared Spectroscopy (FTIR).

Results and Discussion

The morphology of the InN nanostructures is found strongly affected by the growth pressure. Figure 1 shows a set of SEM images of InN nanostructures prepared at different chamber pressures: (a) 18 Torr; (b) 60 Torr; (c) 200 Torr; and (d) 760 Torr. The indium source temperature was 750 °C and the growth period was 5 h for all four samples. The sample temperature was 600 ± 15 °C. InN nanowires were observed at both the lowest and highest pressure. However, much lower density of the nanowires occurs in the former case. In addition, many particles of irregular shapes can be seen at lower pressures (Fig. 1a, b) with the dimension of the particles varies from hundreds of nanometers to few micrometers, suggesting island growth may dominate at lower pressures. Nevertheless, the columnar morphology shown in Fig. 1b may later lead to 1D growth as suggested by other reports [12]. No InN nanowires were obtained at the intermediate pressures of 60–200 Torr. Some sponge-like nanostructures appeared as the chamber pressure was increased to near or above 200 Torr (Fig. 1c) before InN nanowires (also with some nanobelts visible at the lower temperature end) formed at $\sim$760 Torr (Fig. 1d). This result suggests that the chamber pressure plays an important role in initiation of the InN nanowires. Despite the differences in morphology, all four nanostructures in Fig. 1 have predominantly the same wurtzite InN phase according to their XRD spectra. This suggests that the pressure may mostly affect the nucleation morphology of the InN nanostructure via varying the mean free path and hence the interaction of In and N in the vapor and with substrates.

To understand how the initial growth morphology forms and how it correlates with the morphology of the resulted InN nanostructure, a series of samples were prepared at $\sim$760 Torr pressure in three growth temperature zones (i)–(iii) as shown in Rows (i)–(iii) of Fig. 2 respectively, for different durations of (a) 30 min; (b) 40 min; (c) 50 min; and (d) 5 h. Zones (i), (ii) and (iii) were, respectively, 11.5–12.5, 12.5–14.0 and 14.0–15.2 cm away from the indium source. The source temperature was 750 °C. The sample temperature was, respectively, 600 ± 15 °C in Zone (i), 560 ± 20 °C in Zone (ii), and 490 ± 50 °C in Zone (iii). Column (d) compares the morphology difference in InN nanostructures after 5 h in the three different temperature zones. High density InN nanowires were obtained in Zone (i), while microtubes are dominant features in Zone (ii) and

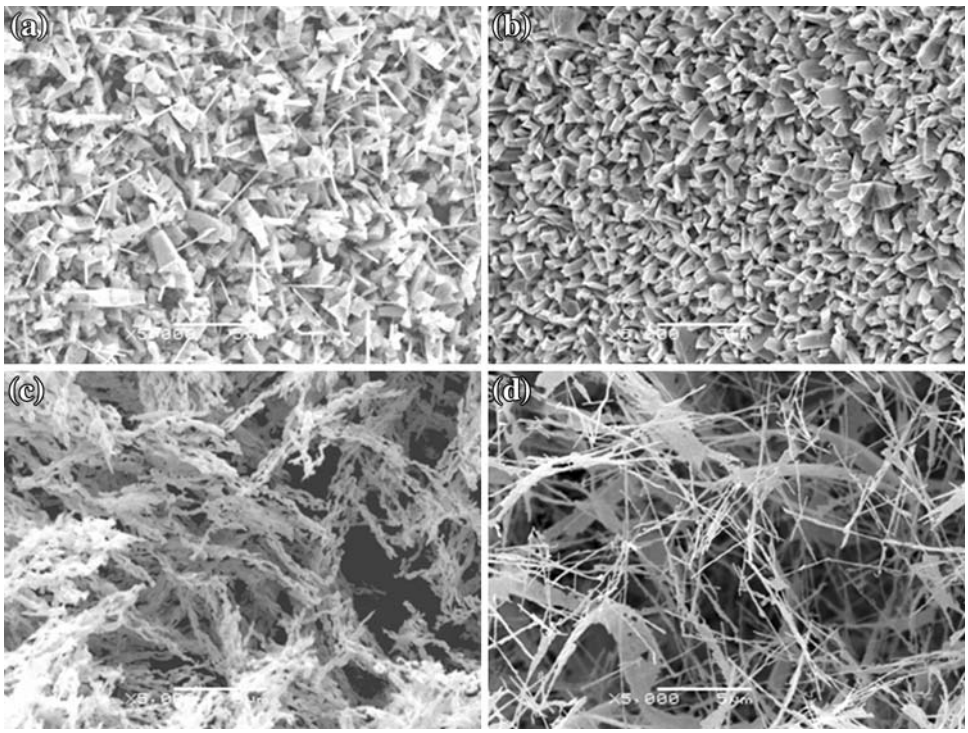

Fig. 1 SEM image of InN nanostructure samples prepared at a chamber pressure of **a** 18 Torr; **b** 60 Torr; **c** 200 Torr; and **d** 760 Torr, respectively. The *scale bars* are 5 μm

(iii). Although InN nanowires and microtubes were reported earlier by different groups [12, 13], our result suggests they can be obtained by simply varying the growth temperature. It is worth mentioning that the similar InN morphology distribution shifts closer to (farther away from) the center of the furnace when the indium source temperature was decreased (increased) in the temperature range of 650–850 °C. This indicates that it is the sample growth temperature, not the distance between the indium source and the sample that is important in determining the InN nanostructure morphology.

To shed light on how the InN 1D nanostructures of different morphologies initiate at different growth temperatures, the growth was terminated at earlier stages after a short time of growth of few to few tens of minutes. Basically, only well-isolated particles were visible for growth time up to ~30 min (Column (a) of Fig. 2). This is in contrast to the dense layer of connected particles in the low-pressure case (Fig. 1a, b), suggesting much enhanced mobility of InN_x on the substrate at higher growth pressure. We speculate a wetting layer of In-rich InN_x is formed at the very initial growth stage, which facilitates material

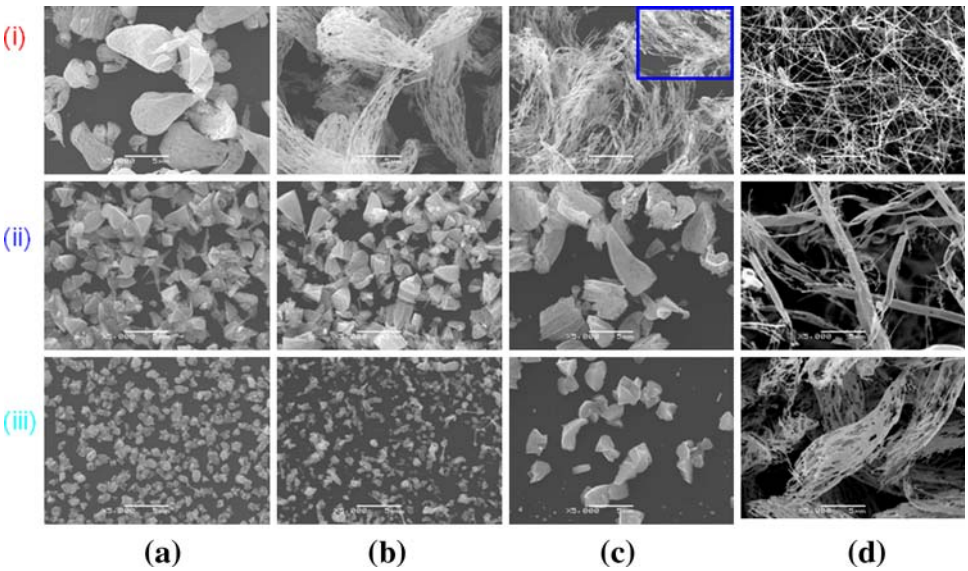

Fig. 2 SEM images of InN samples taken in different growth temperature zones [different rows: (*i*) 11.5–12.5 cm (*ii*) 12.5–14.0 cm and (*iii*) 14.0–15.2 cm away from furnace center.] for different growth duration [different column: **a** 30 min; **b** 40 min; **c** 50 min; (d) 5 h]. The *scale bars* are 5 μm

migration and leads to isolated particle formation. This argument is supported by the size increase of the isolated particles with the growth time. The size of the particles is also different in different zones with larger size particles observed in higher temperature zones. In Zone (i), the average dimension of the particles is $\sim 4 \pm 3$ μm while in Zone (iii), $\sim 500 \pm 350$ nm, about one order of magnitude smaller. In addition to the size difference, some distinct difference in particle shapes can also be observed. Although the particles obtained at lower temperatures do not appear to have special shapes, those at the highest temperature in Zone (i) have a cone or pyramid shape. XRD θ-2θ scans of such cones show no peak through 20–70 degrees, indicating the cones are in amorphous phase. EDS analysis of the cone composition shown in Fig. 3 (black) suggests InN_x phase in the cone. Interestingly, the EDS spectrum of InN nanowires (red) in Fig. 2(id) overlays more or less on that of the cone, suggesting that initiation of InN nanowires most probably occurs as the consequence of the crystallites of InN nucleating and evolving from liquid phase of amorphous InN_x microcones that later disappeared. At longer growth duration of 40–50 min as shown in column (b) and (c), the cones in Zone (i) grew mostly along the cone axial direction with 1D features emerging from the base of the cone. At even longer time, these 1D features developed into InN nanowires, with growth rate on the order of micron per minute (inset of Fig. 2(ic) and Fig. 2(id)]. Interestingly, the particles in Zone (ii) and (iii) grew bigger with longer growth duration and many cone-shaped particles became visible [for example, Fig. 2(iic)]. One may speculate that the slightly lower temperature, such as in Zone (ii), may result in slower and less efficient development of a similar procedure of particle-to-InN nanostructure, which may be attributed to lower mobility and hence lower accumulation rate of indium and nitrogen on particles and lower reaction rate between indium and nitrogen to form InN. Nevertheless, the morphology of lower temperature grown InN nanostructure differs from that obtained in Zone (i), suggesting the nucleation and evolution of InN crystallites are sensitively dictated by the growth temperature. Nevertheless, this result suggests two different modes of InN nanowire growth with (at higher pressure) and without (at lower pressure) facilitation of liquid InN_x phase.

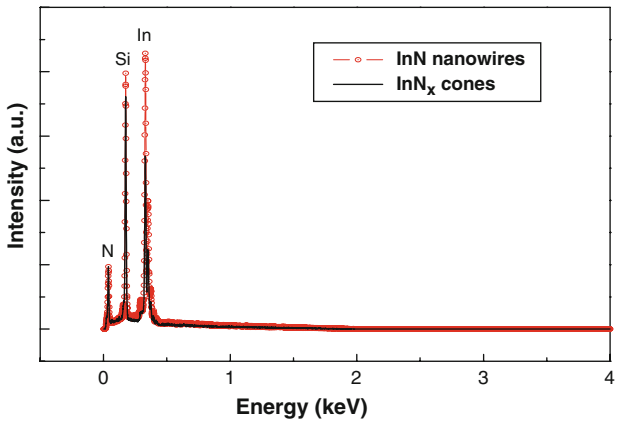

Fig. 3 EDS spectra for InN_x cone (*black*) and InN nanowires (*red*), respectively. A relatively lower indium signal in InN_x microcones is probably due to nonuniform radial distribution of In and N in the micron-size cone with more N expected from core surface attachment of N in vapor. Due to the short penetration of electron beam used for EDS, the surface signals may be emphasized when compared to that of the inner part of the cone

The XRD and FTIR studies have revealed that the three InN nanostructures shown in Column (d) of Fig. 2 with different morphologies have qualitatively similar crystalline structure and E_g (Fig. 4). The red curves were taken on the sample in Fig. 2(id), blue ones on that in Fig. 2(iid), and cyan ones on that in Fig. 2(iiid). The same set of major peaks was observed in XRD θ-2θ spectra for the three samples (Fig. 4a) while much higher peak intensity was observed in the InN nanowire sample (red) grown in Zone (i). The observed diffraction peaks can be indexed to (100), (002), (101), (102), (110), (112), and (201) of hexagonal wurtzite phase of InN. The lattice constants were estimated to be $a = 0.354$ nm and $c = 0.570$ nm. No indium oxide peak was observed. This suggests that the growth temperature directly affects the crystalline quality of InN nanostructure. The E_g of all three samples is around 1.18 eV shown in the FTIR spectra (Fig. 4b), showing a clear blue shift relative to the value of 0.7–0.9 eV for InN. A possible reason is the Burstein-Moss shift caused by the high electron concentrations of the InN nanostructures [20, 21], since XRD spectrum shows no oxide incorporation. A similar observation was reported also by Xu et al. [22]. Considering the lower XRD peaks in the microtube samples, it is not surprising that the FTIR peak intensity for these two samples is also significant lower than that of InN nanowire sample, suggesting the growth temperature around 600 °C is necessary to reach high crystalline quality in InN nanowires.

The morphology and crystalline structure of the InN nanowires were further examined using SEM and TEM and the results are summarized in Fig. 5. Figure 5a shows a magnified SEM image of the InN nanowires shown previously in Fig. 2(id), while Fig. 5b, c shows TEM images of single InN nanowires fabricated under a similar condition. The nanowire diameters were in the range of 80–150 nm with length up to tens of microns. The surface morphology of the nanowires appears relatively smooth as shown in Fig. 5a while a closer examination shown in Fig. 5b and c reveals the contoured edges of the nanowires. HRTEM analysis (Fig. 5c) reveals single-crystalline structure of the InN nanowires. An amorphous sheath with

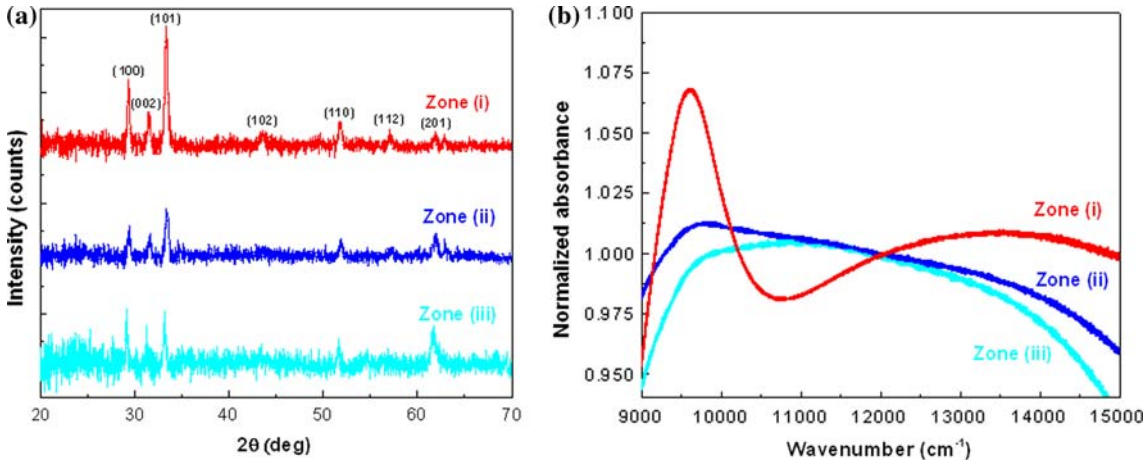

Fig. 4 **a** XRD θ-2θ spectra and **b** FTIR spectra normalized to the respective absorbance at 12,000 cm^{-1} of InN nanostructures shown in the **d** column of Fig. 2

thickness of 0.7–1.7 nm can be clearly seen. The selected area electron diffraction (SAED) pattern (Fig. 5d) confirms the hexagonal structure with lattice constants of approximately $a = 0.365$ nm and $c = 0.584$ nm, consistent with the XRD result shown in Fig. 4a. It is interesting to note that no indium droplets at the tips of nanowires are visible, which is consistent with earlier report by Mohammad and Xu et al. [18, 22] and indicates that the self-catalyzed growth of InN nanowires differs from the VLS growth where a metallic tip initiates and serves as the interface for nanowire growth.

Although a thorough understanding of the self-catalysis process requires a more systematic study, this experiment has provided several important clues on the growth mechanism of InN nanostructures in a CVD process. Based on these, we propose a model shown schematically in

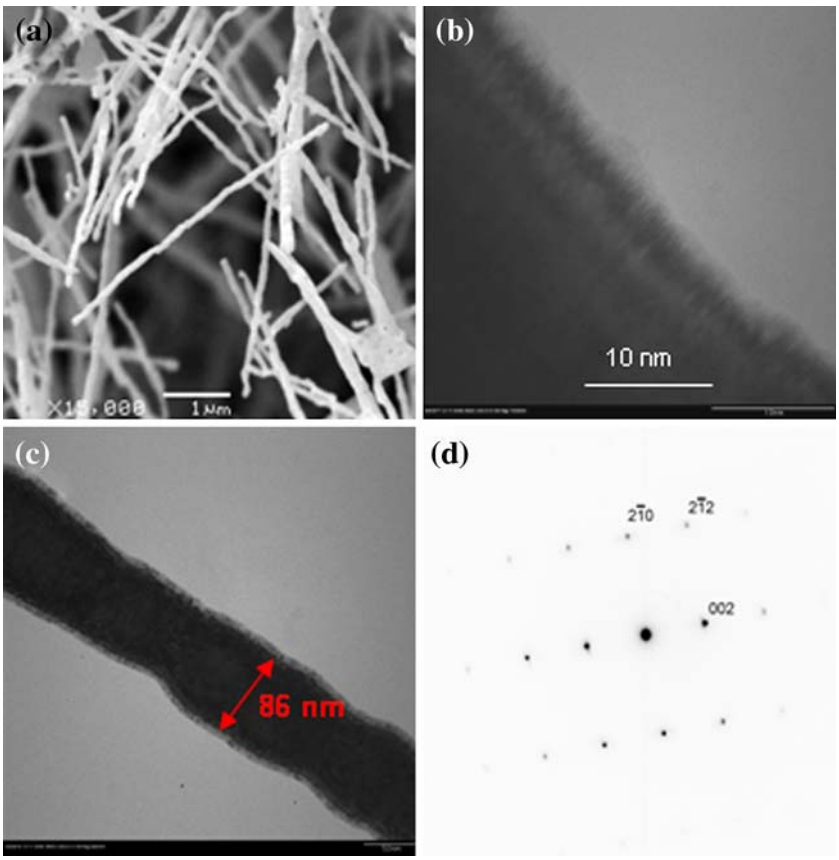

Fig. 5 **a** SEM image of InN nanowires. **b**, **c** TEM images of InN nanowires and **d** shows the SEAD pattern

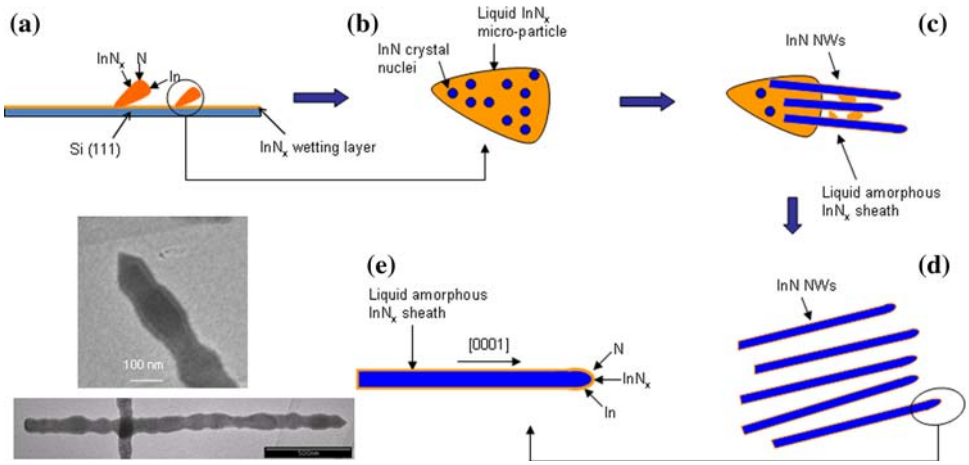

Fig. 6 Schematic description of nucleation and evolution of InN nanowires in the self-catalyzed growth process. **a** Formation of liquid InN_x microparticles. **b** Nucleation of multiple InN crystallites inside the liquid InN_x microparticles. **c** Anisotropic growth of InN nanowires from the crystallites along [0001] direction out of the InN_x microparticles. **d** Further growth of InN nanowires with the help of amorphous InN_x sheath in liquid phase after InN_x microparticles disappeared and **e** a magnified view of one InN nanowire, inset showing the TEM image of InN nanowires with a sharp tip wrapped around an amorphous layer

Fig. 6. First of all, the amorphous InN_x microparticles that appear at the initial stage of growth play a critical role in facilitating absorption of nitrogen and indium in vapor phase and nucleation of InN crystallites. We speculate that similar to catalyst-free growth of GaN nanowires [23], a thin InN_x wetting layer forms on the surface of substrate followed by segregation of the liquid InN_x of high mobility to form particles as schematically showing in Fig. 6a. These InN_x microparticles are most probably in liquid phase since they disappear after InN nanowires form. Secondly, 1D growth of the InN nanostructures from the nucleated InN crystallites is mainly a consequence of anisotropic growth rate of different crystalline orientations in InN. This argument is supported by the apparent favored growth along the [0001] direction. As noted in the lattice fringes in Fig. 5c, the measured spacing $d \sim 0.29$ nm (along the axial direction of the InN nanowire) is consistent with the (0002) plane separation for hexagonal InN. It should be mentioned that the preferential growth orientation along [0001] [19, 22, 24] and $[11\bar{2}0]$ [10, 11] has been observed previously. The observation of bundles of InN nanowires protruding out of an InN_x microparticle further supports the argument that the microparticle is in liquid phase, which allows nucleation of multiple InN crystallites and alignment of the 1D InN nanostructures when anisotropic growth prevails as described in Fig. 6b and c. Finally, the liquid phase microparticle may evolve into the sheath of the fast growing InN nanowires as shown schematically in Fig. 6d and e. The nanowire growth continues at the tip along the fast growth direction of [0001]. This is similar to the oxide-assisted growth of other semiconductor nanowires [25–27] in which an amorphous oxide sheath in the liquid phase allows absorption of relevant semiconductor elements in the vapor and diffusion afterward to facilitate nanowire growth. This argument is supported by the TEM observation of an amorphous sheath around the InN nanowires in Fig. 5b and c. Since different InN nanostructure morphology was observed in different growth zones, the initial nucleation of InN crystallites, especially their crystalline quality, dimension, and geometry shapes, may be dictated by the growth temperature and could lead to different morphology of the resulted InN nanostructures. Particularly, thinner nanowires could be obtained by reducing crystallite dimension and/or suppressing nanowire lateral growth by modification of growth parameters. Further study on the correlation of the growth parameters and the morphology of the 1D InN nanostructures is important to reach control of the physical properties of the InN nanostructures.

Conclusion

In conclusion, we have investigated the InN nanowire nucleation and evolution in the self-catalyzed growth process in the processing window identified favorable for InN nanowire growth. At high growth pressures $\sim$760 Torr, a liquid InN_x wetting layer was found to play a critical role. Quench at the early stage of the growth revealed that isolated amorphous InN_x microparticles of cone shape form in the initial stage of the growth. InN crystallites later formed inside the cone may experience highly anisotropic growth along the favorable [0001] orientation, resulting in InN nanowire bundles protruding out from the microparticle. The microparticles are most probably in liquid phase, which is supported by the observation of disappearance of

the microparticles after InN nanowires form and the alignment of the InN nanowires protruding out from the same microparticle. The liquid phase microparticle may eventually evolve into the amorphous sheath, which serves as an interface between growing InN nanowires and incoming vapors of indium and nitrogen and supports fast growth of InN nanowires in a similar way to the oxide sheath in the oxide-assisted growth of other semiconductor nanowires such as Si.

Acknowledgments This research was supported in part by DOE, NSF, and AFOSR.

References

1. V.Yu. Davydov, A.A. Klochikhin, R.P. Seisyan, V.V. Emtsev, S.V. Ivanov, F. Bechstedt, J. Furthmuller, H. Harima, A.V. Mudryi, J. Aderhold, O. Semchinova, J. Graul, Phys. Status Solidi **229**, R1 (2002)
2. J. Wu, W. Walukiewicz, K.M. Yu, J.W. Ager III, E.E. Haller, H. Lu, W.J. Schaff, Y. Saito, Y. Nanishi, Appl. Phys. Lett. **80**, 3967 (2002)
3. T. Matsuoka, H. Okamoto, M. Nakao, H. Harima, E. Kurimoto, Appl. Phys. Lett. **81**, 1246 (2002)
4. S.N. Mohammad, H. Morkoc, Prog. Quantum Electron. **20**, 361 (1996)
5. S.K. O'Leary, B.E. Foutz, M.S. Shur, U.V. Bhapkar, L.F. Eastman, J. Appl. Phys. **83**, 826 (1997)
6. E. Bellotti, B.F. Brennan, J.D. Albrecht, L.F. Eastman, J. Appl. Phys. **85**, 916 (1999)
7. B.E. Foutz, S.K. O'Leary, M.S. Shur, L.F. Eastman, J. Appl. Phys. **85**, 7727 (1999)
8. E.P.A.M. Bakkers, M.T. Borgstrom, M.A. Verheijen, MRS Bull. **32**, 117 (2007)
9. K.A. Dick, K. Deppert, L.S. Karlsson, M.W. Larsson, W. Seifert, L.R. Wallenberg, L. Samuelson, MRS Bull. **32**, 127 (2007)
10. C.H. Liang, L.C. Chen, J.S. Hwang, K.H. Chen, Y.T. Hung, Y.F. Chen, Appl. Phys. Lett. **81**, 22 (2002)
11. S. Vaddiraju, A. Mohite, A. Chin, M. Meyyappan, G. Sumanasekera, B.W. Alphenaar, M.K. Sunkara, Nano Lett. **5**, 1625 (2005)
12. T. Stoica, R. Meijers, R. Calarco, T. Richter, H. Lüth, J. Cryst. Growth **290**, 241 (2006)
13. S. Luo, W. Zhou, W. Wang, Z. Zhang, L. Liu, X. Dou, J. Wang, X. Zhao, D. Liu, Y. Gao, L. Song, Y. Xiang, J. Zhou, S. Xie, Appl. Phys. Lett. **87**, 063109 (2005)
14. J. Zhang, L. Zhang, X. Peng, X.J. Wang, Mater. Chem. **12**, 802 (2002)
15. Y. Wu, P. Yang, Chem. Mater. **12**, 605 (2000)
16. M.H. Huang, Y. Wu, H. Feick, E. Webber, P. Yang, Adv. Mater. **13**, 113 (2000)
17. A.M. Morales, C.M. Lieber, Science **279**, 208 (1998)
18. S.N. Mohammad, J. Chem. Phys. **127**, 244702 (2007)
19. M.C. Johnson, C.J. Lee, E.D. Bourret-Courchesne, S.L. Konsek, S. Aloni, W.Q. Han, A. Zettl, Appl. Phys. Lett. **85**, 5670 (2004)
20. J. Wu, W. Walukiewicz, S.X. Li, R. Armitage, J.C. Ho, E.R. Weber, E.E. Haller, H. Lu, W.J. Schaff, A. Barcz, R. Jakiela, Appl. Phys. Lett. **84**, 2805 (2004)
21. V.M. Naik, R. Naik, D.B. Haddad, J.S. Thakur, G.W. Auner, H. Lu, W.J. Schaff, Appl. Phys. Lett. **86**, 201913 (2005)
22. H.Y. Xu, Z. Liu, X.T. Zhang, S.K. Hark, Appl. Phys. Lett. **90**, 113105 (2007)
23. T. Stoica, E. Sutter, R.J. Meijers, R.K. Debnath, R. Calarco, H. Lüth, D. Grützmacher, Small **4**, 751 (2008)
24. D. Moore, Z.L. Wang, J. Mater. Chem. **16**, 3898 (2006)
25. S.T. Lee, N. Wang, Y.F. Zhang, Y.H. Tang, Mater. Res. Bull. **24**, 36 (1999)
26. R.Q. Zhang, Y. Lifshitz, S.T. Lee, Adv. Mater. **15**, 635 (2003)
27. R.Q. Zhang, M.W. Zhao, S.T. Lee, Phys. Rev. Lett. **93**, 095503 (2004)